Functional Organization of Owl Monkey Lateral Geniculate Nucleus and Visual Cortex

LAWRENCE P. O'KEEFE,[1,2] JONATHAN B. LEVITT,[1] DANIEL C. KIPER,[1,2] ROBERT M. SHAPLEY,[1] AND J. ANTHONY MOVSHON[1,2]

[1]Center for Neural Science and [2]Howard Hughes Medical Institute, New York University, New York 10003-6621

O'Keefe, Lawrence P., Jonathan B. Levitt, Daniel C. Kiper, Robert M. Shapley, and J. Anthony Movshon. Functional organization of owl monkey lateral geniculate nucleus and visual cortex. *J. Neurophysiol.* 80: 594–609, 1998. The nocturnal, New World owl monkey (*Aotus trivirgatus*) has a rod-dominated retina containing only a single cone type, supporting only the most rudimentary color vision. However, it does have well-developed magnocellular (M) and parvocellular (P) retinostriate pathways and striate cortical architecture [as defined by the pattern of staining for the activity-dependent marker cytochrome oxidase (CO)] similar to that seen in diurnal primates. We recorded from single neurons in anesthetized, paralyzed owl monkeys using drifting, luminance-modulated sinusoidal gratings, comparing receptive field properties of M and P neurons in the lateral geniculate nucleus and in V1 neurons assigned to CO "blob," "edge," and "interblob" regions and across layers. Tested with achromatic stimuli, the receptive field properties of M and P neurons resembled those reported for other primates. The contrast sensitivity of P cells in the owl monkey was similar to that of P cells in the macaque, but the contrast sensitivities of M cells in the owl monkey were markedly lower than those in the macaque. We found no differences in eye dominance, orientation, or spatial frequency tuning, temporal frequency tuning, or contrast response for V1 neurons assigned to different CO compartments; we did find fewer direction-selective cells in blobs than in other compartments. We noticed laminar differences in some receptive field properties. Cells in the supragranular layers preferred higher spatial and lower temporal frequencies and had lower contrast sensitivity than did cells in the granular and infragranular layers. Our data suggest that the receptive field properties across functional compartments in V1 are quite homogeneous, inconsistent with the notion that CO blobs anatomically segregate signals from different functional "streams."

INTRODUCTION

The primate visual system contains several separate, parallel pathways originating in the retina (see Shapley 1992). These pathways remain segregated in the lateral geniculate nucleus (LGN) and in the pattern of projections to the primary visual cortex (V1) (see Casagrande and Kaas 1994 for a recent review). Neurons in the parvocellular (P) pathway typically have much lower sensitivity to luminance contrast and much higher sensitivity to chromatic contrast than do neurons in the magnocellular (M) pathway. Furthermore, at any eccentricity, the neurons with the best spatial resolution belong to the P pathway, whereas those with the best temporal resolution belong to the M pathway. (Derrington and Lennie 1984; Derrington et al. 1984; Kaplan and Shapley 1982, 1986; Levitt et al. 1997; Schiller and Malpeli 1978;

Spear et al. 1994; Wiesel and Hubel 1966). Visual information may also be segregated within the primary visual cortex and in its projections to extrastriate areas (Livingstone and Hubel 1988; Merigan and Maunsell 1993), though it is unlikely that this segregation reflects that of the M and P pathways; there is anatomic (Callaway and Wiser 1996; Lachica et al. 1992, 1993; Tootell et al. 1988b; Yoshioka et al. 1994) and physiological (Malpeli et al. 1981; Nealey and Maunsell 1994; Sawatari and Callaway 1996) evidence for mixing of M and P signals at the level of V1.

Tangential organization in visual cortex was suggested by Hubel and Wiesel's (1968, 1974) observation of a regular sequence of preferred orientations on long electrode penetrations through the cortex. They proposed that the visual cortex was organized into hypercolumns processing all possible orientations for both eyes (Hubel and Wiesel 1977). A possible anatomic marker for the tangential organization of the visual cortex is the metabolic enzyme cytochrome oxidase (Wong-Riley 1979; and see Wong-Riley 1994 for a review), which forms patches in the superficial layers known variously as "puffs" or "blobs" (Horton and Hubel 1981; Humphrey and Hendrickson 1983). Cytochrome oxidase (CO) blobs are a prominent feature of the visual cortex in all primates so far examined (Horton 1984). The CO blobs may mark populations of neurons with visual properties that are qualitatively and quantitatively different from neurons outside of blobs (Livingstone and Hubel 1988). Cells in blobs in macaque have been reported to be color-selective, monocular, nonoriented (Livingstone and Hubel 1984; Tootell et al. 1988a; Ts'o and Gilbert 1988), and selective for low spatial frequencies (Born and Tootell 1991; Edwards et al. 1995; Silverman et al. 1989; Tootell et al. 1988c) and reported as having high contrast sensitivity (Edwards et al. 1995; Hubel and Livingstone 1990) when compared with cells in interblob regions. It is unlikely that the blob system marks a color pathway in all primates because blobs are well defined in primates that lack color vision (Condo and Casagrande 1990; Horton 1984; Tootell et al. 1985). Furthermore, recent studies in macaque visual cortex suggest that the receptive field properties inside and outside of blobs are less distinct than was originally suggested (e.g., Edwards et al. 1995; Lennie et al. 1990; Leventhal et al. 1995).

We studied the relationship between receptive field properties and CO activity in the nocturnal New World owl monkey (*Aotus trivirgatus*). We chose the owl monkey because it possesses a well-defined CO blob system but lacks two of the features thought to be associated with the blob system,

namely color vision and well-defined eye dominance columns. The owl monkey has a rod-dominated retina (Ogden 1975; Wikler and Rakic 1990) with a single cone type (Jacobs et al. 1993) that supports only the most rudimentary color vision (Jacobs 1977; Jacobs et al. 1993). Its retina contains morphological M- and P-type ganglion cells (Silveira et al. 1994), and its lateral geniculate nucleus has a lamination pattern similar to other monkeys, consisting of two magnocellular and two (or more) parvocellular layers (Diamond et al. 1985; Jones 1966a,b; Kaas et al. 1978). The receptive field properties of neurons in the owl monkey LGN appear to reflect the anatomic segregation as they do in other primates (Sherman et al. 1976). The laminar pattern of projections from the magno- and parvocellular LGN to V1 are generally similar to those of other primates (Diamond et al. 1985), but the eye dominance columns seen in Old World monkeys and larger New World monkeys are barely discernible (Diamond et al. 1985; Kaas et al. 1976; Rowe et al. 1978). The topography of the primary visual cortex and several extrastriate cortical areas have been well studied (Allman and Kaas 1971a,b, 1974a,b, 1975), but the receptive field properties of individual neurons in V1 have not been studied in detail, particularly with respect to the CO blobs. We studied the orientation/direction tuning (in V1) and the spatial and temporal frequency tuning and contrast response (in the LGN and V1) of owl monkey neurons using achromatic drifting sinusoidal gratings. We chose these measures for convenient comparison with macaque and as a means of following the signature of the M and P pathways into V1.

Because the properties of neurons in CO blobs are thought to be related to patterns of M and P input, it was crucial to determine if M and P cells in the owl monkey could be distinguished in the same way that they are in other primates. We found that M and P cells had receptive field properties broadly similar to those of other primates. We examined the receptive field properties of V1 neurons located in different CO compartments and across layers. We also found the receptive field properties of owl monkey V1 neurons to be similar to those of other primates. We found that receptive field properties did not vary across CO compartments but that some receptive field properties did vary across layers. We conclude that in the owl monkey, the CO blob system is not an anatomic marker for a strongly segregated parallel stream of cortical information processing.

METHODS

Seven adult owl monkeys (*A. trivirgatus,* weights: 0.6–1.0 kg) were prepared for single-unit recording using methods similar to those we use in macaques (Levitt et al. 1994). In one monkey, recordings were made in the LGN, while in the remaining monkeys, recordings were made on long, tangential penetrations through V1.

Surgical preparation and maintenance

Animals were premedicated with atropine (0.05 mg/kg) and acepromazine (0.05 mg/kg) or diazepam (Valium: 0.05 mg/kg). After induction of anesthesia with intramuscular injections of ketamine HCl (Vetalar: 8–12 mg/kg), cannulae were inserted into the trachea and the saphenous veins, the animal's head was fixed in a stereotaxic frame, and surgery was continued under intravenous

anesthesia. In two experiments, we used continuous infusion of sodium thiopental (Pentothal: $1-2$ mg$\cdot$kg$^{-1}\cdot$h^{-1}) or urethan (10 mg$\cdot$kg$^{-1}\cdot$h^{-1}) for anesthesia. Later, we used the opiate anesthetic sufentanil citrate (Sufenta: $4-8$ mg$\cdot$kg$^{-1}\cdot$h^{-1}). Infusion of the surgical anesthetic continued throughout the recordings. We noticed no obvious difference in the properties of recorded units under the different anesthetic regimes.

To minimize eye movements, paralysis was maintained with an infusion of vecuronium bromide (Norcuron: 0.1 mg$\cdot$kg$^{-1}\cdot$h^{-1}) in an electrolyte solution (Normosol) with dextrose (2–5 ml/h). Animals were ventilated artificially with room air or a mixture of 50–70% N_2O in O_2. Peak expired P_{CO_2} was maintained near 4% by adjusting the tidal volume of the ventilator. Rectal temperature was kept near 37°C with a thermostatically controlled heating pad. Animals received daily injections of a broad-spectrum antibiotic (Bicillin: 150,000 U) to prevent infection, as well as dexamethasone (Decadron: 0.5 mg/kg) to prevent cerebral edema. Electrocardiograms, electroencephalograms, autonomic signs, and rectal temperature were monitored continuously to ensure the adequacy of anesthesia and the soundness of the animal's physiological condition.

Tungsten-in-glass microelectrodes (Merrill and Ainsworth 1972) were introduced by a hydraulic microdrive through a small guide needle into the portions of the LGN or V1 representing the central visual field. After the electrode was in place in the cortex, the exposed dura was covered with warm agar. Action potentials were conventionally amplified, displayed, and played over an audio monitor. The recording sessions lasted between 36 and 72 h.

Physiological optics

The pupils were dilated, and accommodation was paralyzed with topical atropine, and the corneas were protected with +2D gas-permeable hard contact lenses. Supplementary lenses were chosen to make the retinas conjugate with the display screen as judged by optimizing the visual responses of recorded units. Contact lenses were removed periodically for cleaning. At this time, the eyes were rinsed with saline and infiltrated with a few drops of ophthalmic antibiotic solution (Gentamicin). At least once a day, the locations of the area centrales were recorded using a reversible ophthalmoscope.

Characterization of receptive fields

We initially mapped the receptive fields of single neurons by hand on a tangent screen using black-and-white geometric targets. For each neuron, we recorded the location and size of the neuron's minimum response fields and determined its selectivity for the orientation and size of stimuli. Ocular dominance was assessed qualitatively using the seven-point scale of Hubel and Wiesel (1962).

We used a mirror to place the preferred eye's receptive field on the face of a display monitor that subtended 7–8°. Stimuli were luminance-modulated drifting sinusoidal gratings generated by a TrueVision ATVista board (582 × 752 pixels, 106 Hz interlaced) and displayed on gamma-corrected monitors, initially a Barco 7650 (mean luminance 36 cd/m^2), later a Nanao T560i (mean luminance 72 cd/m^2). Before beginning quantitative measurements, we optimized stimulus size, orientation, and drift rate by listening to the neuron's response over the audio monitor. For nearly all LGN neurons, stimuli occupied the full screen, were horizontally oriented, and drifted downward. For nearly all V1 neurons, stimuli occupied less than the full screen. All quantitative experiments were run under computer control, and consisted of three to four repetitions of a pseudorandom sequence of stimuli, each lasting ~4 s separated by a 1- to 2-s interval of mean luminance. The computer stored the arrival times of individual action potentials.

These were assembled into conventional peristimulus time histograms and rasters, and were Fourier-analyzed to determine the mean (DC), first harmonic (F1), and temporal phase of each response.

Reconstruction of recording sites

At the end of each electrode penetration, small electrolytic lesions ($2 \mu A$, 2 s, tip negative) were made along the electrode track to facilitate reconstruction. In all cases, we selected lesion sites characterized by particular visual response properties and verified that these properties were still in evidence before making lesions. Our laboratory has demonstrated the accuracy of this technique in recordings from the LGN and V1 of macaque monkeys, where the relationship between receptive field properties and laminar borders is well documented. In those experiments, we noted the depths of eye dominance changes when recording from the LGN and the depths of the brisk unoriented activity characteristic of layer 4C when recording from V1. At the end of each penetration, we retracted the electrode to each of the previously noted depths, verified the eye switch or laminar position, and made a lesion. The depths of borders encountered while retracting the electrode never differed by more than a few tens of micrometers from those initially noted, and subsequent histology showed that lesions were invariably located on borders between LGN or cortical layers. We are confident that the technique yields similar location accuracy in the owl monkey. Monkeys were killed with an overdose of Nembutal and perfused transcardially with saline followed by 4% paraformaldehyde. The brains were postfixed in paraformaldehyde, sunk in 30% sucrose, and sectioned at 40 μm on a freezing microtome. Alternate sections were stained for CO, dihydronicotinamide adenine dinucleotide phosphate diaphorase (NADPH-d), and cresyl violet following methods described in Gegenfurtner et al. (1996). The pattern of NADPH-d activity has been shown to overlap that of CO in macaque V1 (Sandell 1986) and V2 (Gegenfurtner et al. 1996) and owl monkey V1 (Wiencken and Casagrande 1996). In cases where CO staining was weak, we used NADPH-d staining to identify blobs. We made complete, three-dimensional reconstructions of the electrode tracks for six of the eight recorded hemispheres; the quality of the histological material from the remaining two hemispheres was deemed inadequate. The reconstructions were based on camera lucida drawings of neighboring Nissl and CO-stained sections containing the electrode tracks. Boundaries of CO-rich regions, laminar borders, and blood vessels serving as fiducial marks were drawn by hand, and the drawings were stacked by aligning blood vessels. Recording sites along the three-dimensional trajectory of the track were marked on the composite drawing. We defined cortical layers based on the descriptions and illustrations in Diamond et al. (1985) but did not subdivide layer 3. Instead, we combined in one group all cells in residing in layers 2 and 3. Each cell was given a laminar assignment, and if it resided in the supragranular layers, we attempted to assign it to one of three compartments; within (blob), on the edge of (edge), or in between (inter) CO-rich regions. We assigned a cell to a compartment only if its location could be determined unambiguously; as a result, 29 layer 2/3 cells were excluded from the compartment analysis. For each of the 71 layer 2/3 neurons assigned to a compartment, we measured the distance to the nearest blob center (based on the 3-D reconstructions).

Data analysis and statistics

For all quantitative measures (orientation, spatial and temporal frequency tuning, and contrast response), we fitted appropriate descriptive functions to the response data using techniques described in Levitt et al. (1994). From the fits, we derived parameters of interest described in the following sections. When describing parameter distributions, we use the median unless noted otherwise. We used the nonparametric Mann-Whitney U test to compare distributions of parameters between pairs of neuron groups. We used the nonparametric Kruskal-Wallis analysis of variance (ANOVA) of ranks to compare distributions of parameters for three or more groups.

RESULTS

We recorded quantitative data from 211 V1 cells and 50 LGN cells. Receptive fields of recorded cells lay within 5° (V1) or 10° (LGN) of the area centralis.

Receptive field properties of LGN neurons

Of the 50 cells recorded in the LGN, 23 were assigned to the P layers, and 21 in the M layers. We could not make laminar assignments for four LGN neurons, which were excluded from further analysis. We were unable to isolate single units between the principal layers, although we did occasionally encounter long interlaminar zones where we could evoke multiunit activity with visual targets. Sherman et al. (1976) reported similar zones in their study of owl monkey LGN. The receptive fields of our sample of P cells were, on average closer (mean 3.0, range 1.0–7.6°) to the area centralis than those for our sample of M cells (mean 7.5, range 2.2–12.6°).

DESCRIPTION OF MEASUREMENTS. Figure 1, *A–C,* shows example data collected from a neuron in the parvicellular layers of the LGN. The receptive field was located 1° from the area centralis. Figure 1*A* shows the neuron's spatial frequency tuning. We typically presented seven spatial frequencies in octave steps spanning a range of 0.125–8.0 cycles/deg. The figure also shows (———) the best fitting difference-of-Gaussians function (Enroth-Cugell and Robson 1966; Linsenmeier et al. 1982) of the form

$$R = k_c(e^{-(f/f_c)^2} - k_s e^{-(f/f_s)^2})$$

where R is response, k_c is the strength of the center mechanism, k_s is the relative strength of the surround mechanism, and f_c and f_s are the characteristic spatial frequencies of the center and surround mechanisms. We found that our measures provided good estimates of center frequencies but not of surround frequencies, which depend on measurements made at very low spatial frequencies. The data in Fig. 1*A* yielded an estimated center frequency of 5.0 cycles/deg, an optimal spatial frequency of ~2.1 cycles/deg and a spatial resolution (the spatial frequency at which the value of the function falls to 1 imp/s) of 9.6 cycles/deg.

Figure 1*B* shows the neuron's temporal frequency (TF) tuning. We presented seven temporal frequencies in octave steps, spanning a range of 0.83–26.5 Hz. We fitted a descriptive function (———) to the data to estimate optimal temporal frequency (~4.0 Hz), temporal frequency cutoff (the temporal frequency at which response drops to one-half of the maximum, 21.8 Hz for this example), and transience [the ratio of the low-frequency response (at a TF 1 decade below optimal TF) to the peak response].

Figure 1*C* shows the neuron's contrast response measured with stimulus contrasts ranging from ~0.008 to 1.0 in octave steps. We fit the data to a function suggested by Robson (1980)
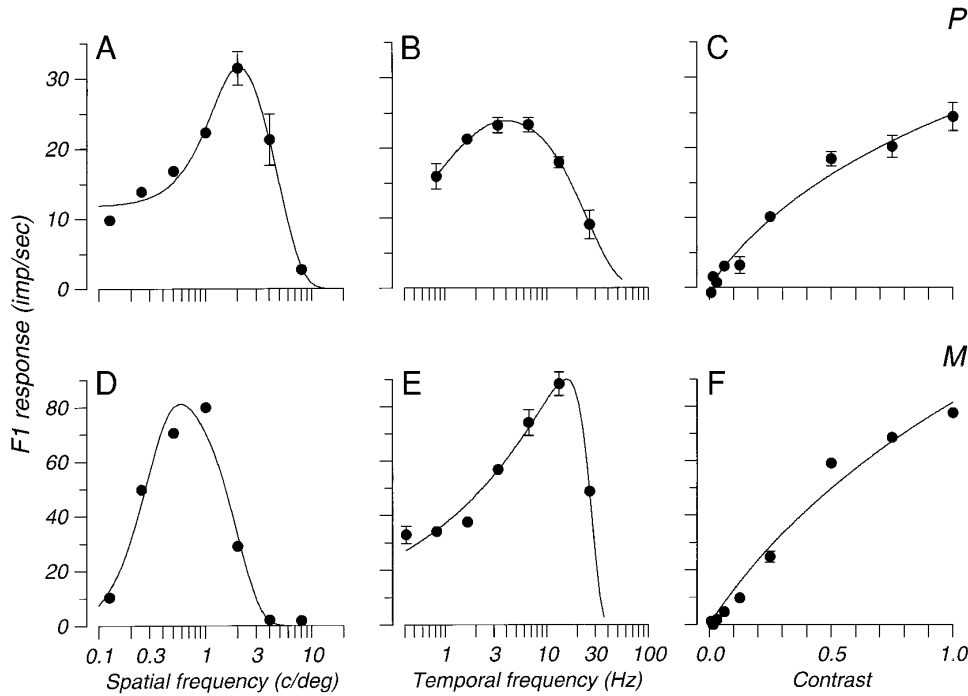
FIG. 1. Receptive field properties of 2 owl monkey LGN neurons. Data are F1 responses, i.e., modulation of firing rate at the stimulus temporal frequency. Error bars are ±1 SE of the mean. ——, fits of descriptive functions—see text for details. *A–C*: parvocellular neuron (P). *A*: spatial frequency tuning. *B*: temporal frequency tuning. *C*: contrast response. *D–F*: magnocellular neuron (M). *D*: spatial frequency tuning. *E*: temporal frequency tuning. *F*: contrast response.

$$R = k \log \left(1 + \frac{C}{C_0} \right)$$

where R is response, k is gain, C is contrast, and C_0 is a saturation constant. We took R to be the component of the response at the phase of the response to the highest contrast to reduce the effect of response variability on the fits (Levitt et al. 1989). We used the fits to estimate peak response and responsivity (sometimes called contrast gain), the initial slope (k/C_0) of the contrast response function in impulses·second^{-1}·contrast^{-1}. Peak response in Fig. 1*C* was 24.8 imp/s and responsivity was 50.9.

Figure 1, *D–F,* shows similar measurements collected from a neuron in a magnocellular layer of the LGN the receptive field of which was centered 10° from the area centralis. Figure 1*D* shows spatial frequency tuning data. This neuron had a lower center frequency (1.4 cycles/deg) and a lower optimal spatial frequency (0.6 cycles/deg) than did the P cell the data of which are shown in Fig. 1*A*. The temporal frequency tuning data for this neuron are shown in Fig. 1*E*. The neuron had a higher optimal (15.6 Hz) and cutoff (27.1 Hz) temporal frequency than its parvocellular counterpart (Fig. 1*B*). Figure 1*F* shows the contrast-response data for this neuron. This cell showed a higher peak response (81.5 imp/s) and greater responsivity (133.6) than did the P cell (Fig. 1*C*).

SPATIAL FREQUENCY TUNING. Table 1 lists estimates of all LGN receptive field parameters. The spatial parameters are characteristic frequency of the center mechanism, weight of the center mechanism, weight of the surround mechanism with respect to the center, and characteristic frequency of the surround with respect to the center. The spatial properties of owl monkey M and P neurons were distinguished best by center frequency. Distributions of center frequency for M and P cells are shown in Fig. 2, *A* and *B*. P cells, on average, had significantly higher center frequencies than did M cells.

Some but not all of this difference is probably due to the greater eccentricity of our M sample.

TEMPORAL FREQUENCY TUNING. Table 1 also lists estimates of LGN temporal parameters: optimal temporal frequency, the high-frequency cutoff, and transience. The temporal properties of M and P cells were best distinguished by optimal temporal frequency. Distributions of this parameter for M and P cells are shown in Fig. 1, *C* and *D*. M cells had, on average, significantly higher optimal temporal frequencies than did P cells.

CONTRAST RESPONSE. Table 1 also shows LGN contrast-response parameters: peak response and responsivity (the ini-

TABLE 1. *Summary of receptive field properties for all cells in our LGN sample*

Property	Magnocellular	Parvocellular	P
Spatial tuning			
Center frequency (f_c), cycles/deg	1.48 (21)	2.97 (22)	**<0.001**
Center strength (k_c)	60.3 (21)	31.6 (22)	**<0.001**
Relative surround strength (k_s)	0.92 (21)	0.64 (22)	**<0.001**
Surround frequency (f_s)	0.26 (21)	0.25 (22)	0.2840
Temporal tuning			
Optimal temporal frequency, Hz	6.4 (20)	4.0 (22)	**<0.001**
High temporal frequency cutoff, Hz	22.6 (21)	16.1 (23)	0.0193
Transience	0.48 (21)	0.36 (23)	0.2020
Contrast response			
Peak response (imp/s)	45.7 (21)	27.5 (22)	**<0.001**
Responsivity, (k/C_0, imp·s^{-1}·contrast^{-1})	70.8 (21)	24.0 (22)	**<0.001**

Values are medians; number of cells in parentheses. *P* values based on the nonparametric Mann-Whitney *U* test; *P* values in bold face indicate significance at the 0.01 level. LGN, lateral geniculate nucleus.
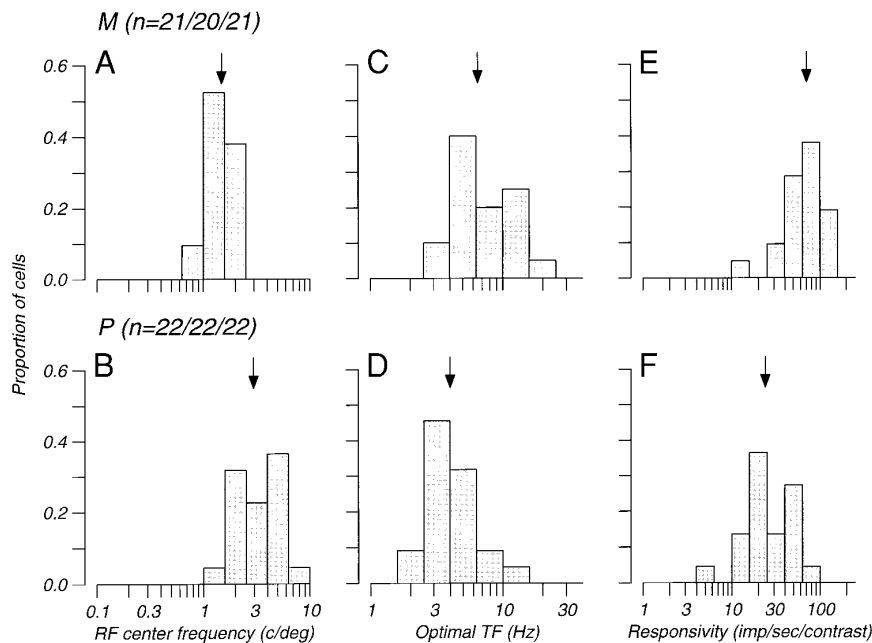
FIG. 2. Distributions of owl monkey LGN receptive field properties. Bars indicate proportion of cells in each bin. Number of cells is indicated in parentheses. →, median of each distribution. *A*: receptive field center radii for M cells. *B*: receptive field center radii for P cells. *C*: optimal temporal frequency for M cells. *D*: optimal temporal frequency for P cells. *E*: responsivity ($\text{imp} \cdot \text{s}^{-1} \cdot \text{contrast}^{-1}$) for M cells. *F*: responsivity ($\text{imp} \cdot \text{s}^{-1} \cdot \text{contrast}^{-1}$) for P cells.

tial slope of the contrast-response function in $\text{imp} \cdot \text{s}^{-1} \cdot \text{contrast}^{-1}$). Figure 2, *E* and *F*, shows distributions of responsivity for M and P cells. M and P cells were distinguished easily on the basis of contrast response—M cells, on average, had significantly higher responsivity and peak responses than did P cells.

These data show that owl monkey M and P cells could be differentiated on the basis of spatial frequency tuning, temporal frequency tuning, and contrast response.

Receptive field properties of V1 neurons

We studied the properties of 211 single neurons in V1, in eight hemispheres from six monkeys. Receptive fields were centered within 5° of the area centralis. We were able to collect quantitative data from all 211 cells and collected full sets of data from 196. We made electrode penetrations nearly tangential to the cortical surface to maximize the probability of sampling from several blob and interblob regions of layers 2/3. Thus our sample is biased heavily toward the upper layers, although we did record from cells throughout the depth of the cortex.

We note that cortical lamination pattern in New World monkeys is defined differently from that of Old World monkeys, particularly the subdivisions of layer 4 (see Casagrande and Kaas 1994; Peters 1994). We have adopted the scheme of Hassler (1994) used for most studies of V1 in New World monkeys, in which layer 4 is defined as having two divisions (A and B) corresponding to the subdivisions of layer 4C in Old World monkeys. Layers 4A and 4B of Old World monkeys thus correspond to subdivisions of layer 3 in New World monkeys. We made coarse laminar assignments for 170 neurons, pooling our samples from the upper (supragranular) layers (2 and 3) the subdivisions of (granular) layer 4, and the (infragranular) lower layers (5 and 6). We assigned 100 cells to layers 2/3, 52 cells to layer 4, and 18 cells to layers 5/6. Our sample of layer 4 was biased to the upper, magnocellular-recipient sublayer 4A; only 4 cells

were assigned to parvocellular-recipient layer 4B. We were unable to make laminar assignments for 41 neurons. We were able to assign 71 of the 100 layer 2/3 cells to one of the three compartments defined by CO or NADPH-d staining patterns; 28 cells were assigned to *blob* compartments, 17 cells were assigned to *edge* compartments, and 26 cells were assigned to *interblob* compartments. Because the sample from each compartment was small, we chose not to subdivide CO compartments on the basis of depth within the supragranular layers.

DESCRIPTION OF MEASUREMENTS. Here we describe our standard measurements for characterizing our sample of V1 neurons. Figure 3, *A–D*, shows data collected from a simple cell in layer 4 of V1. Figure 3*A* shows a polar plot of the neuron's orientation/direction tuning. The solid line through the data is the best fit to a descriptive function used to compute orientation half-width (at half-height) for each cell. We classified a neuron as direction selective if the direction index was ≥0.67 ($R_p \geq 3 * R_n$). This neuron was classified as direction selective with a direction index of 0.81. Figure 3*B* shows the neuron's spatial frequency tuning. The solid line through the data represents the best-fitting function used to derive estimates of optimal spatial frequency, spatial resolution (the spatial frequency at which the value of the function dropped to 1 imp/sec) and spatial frequency bandwidth (in octaves). Figure 3*C* shows the neuron's temporal frequency tuning. The solid line through the data is the best fit from a function used to derive the estimates of optimal temporal frequency, temporal resolution (the temporal frequency at which the value of the function drops to 1 imp/sec), and temporal tuning bandwidth (full width at half-height in octaves.)

Figure 3*D* shows the neuron's contrast response. The contrast-response functions of many owl monkey cortical cells showed saturation at high contrasts (e.g., Fig. 3, *D* and *H*). However, a substantial number of cells (44) did not show saturation even at unit contrast. The solid line through the
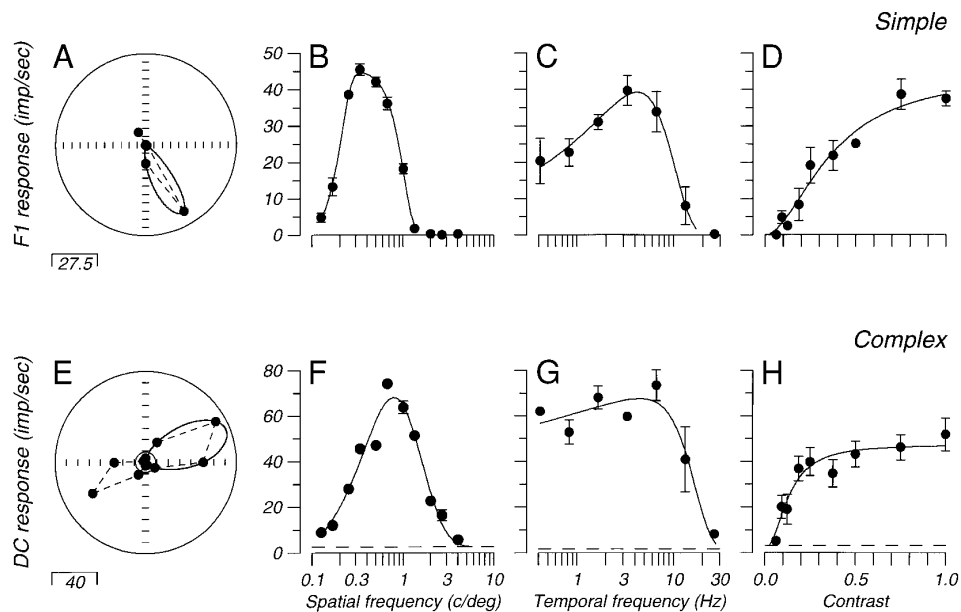
FIG. 3.   Receptive field properties of 2 owl monkey V1 neurons. *A–D*: layer 4 simple cell. Data are the F1 response. *A*: orientation/direction tuning. Neuronal response is represented by distance from the origin, and stimulus direction is represented by polar angle. Data are from 12 directions covering 360° in 30° increments. In later experiments, we measured direction tuning using 16 stimuli in 22.5° increments. We also computed a direction index ($DI = 1 - R_n/R_p$), where R_p is the net response in the preferred direction and R_n is the net response to the opposite (nonpreferred) direction of motion. Index ranges from 0.0 (equal response to the 2 directions) to 1.0 (no response to the nonpreferred direction), or >1.0 if there is suppression in the nonpreferred direction. *B*: spatial frequency tuning. We used 11 stimuli whose spatial frequency varied from 0.125 to 4.0 cycles/deg in half-octave steps, presented at the optimal orientation. *C*: temporal frequency tuning. We measured responses to 7 stimuli at the optimal orientation and spatial frequency whose temporal frequency varied in octave steps from 0.41 to 26.5 Hz. *D*: contrast response. We measured responses to 9–11 spatiotemporally optimal stimuli whose contrast varied in half-octave steps spanning a range of ∼0.01–1.0. *E–H*: layer 4 complex cell. Data are the DC response. *E*: orientation/ direction tuning. *F*: spatial frequency tuning. *G*: temporal frequency tuning. *H*: contrast response. Other conventions as in Fig. 1.

data represents the best fitting hyperbolic ratio (Albrecht and Hamilton, 1982). We used the fit parameters to compute the peak response (response evoked by a unit contrast stimulus) and C_{50} (the contrast that evoked one-half of the peak response). In addition, we computed contrast thresholds for each neuron by compiling neurometric functions from the contrast-response data (Tolhurst et al. 1983). The value of the neurometric function at each contrast represents the probability that an ideal observer could discriminate correctly between that contrast and zero contrast based only on the discharge of the neuron being recorded. We computed maximum likelihood fits of the neurometric functions to a cumulative Weibull distribution and took threshold as the contrast at which the fit value passed through 0.57, a value representing a binomial probability 1 SD above chance performance.

Figure. 3, *E–H,* shows data similarly collected from a complex cell in layer 4 of V1. Response (in the case of complex cells, the DC firing rate in imp/s) is plotted as a function of grating direction (Fig. 3*E*), spatial frequency (Fig. 3*F*), temporal frequency (Fig. 3*G*), and contrast (Fig. 3*H*). This neuron was orientation selective but not direction selective.

Functional architecture of owl monkey visual cortex

Figure 4 shows the reconstruction of an electrode penetration that traversed all layers of V1. Figure 4, *A–C,* shows individual photomicrographs of CO-stained sections, each

of which contains a portion of the electrode track (marked by double arrows). The slightly irregular size, shape, and spacing of the CO blobs is due to the oblique plane of the section. Figure 4*A* shows the upper part of the penetration, including an electrolytic lesion (asterisk) marking the first recording site. The track can be seen exiting a blob in the upper part of layer 2/3. Figure 4*B* shows the electrode track visible in middle potion of layer 2/3 as it enters a second blob. Figure 4*C* shows the remainder of the penetration; asterisks mark lesions at the layer 4/5 border and in layer 6. Figure 4*D* is a montage of these sections, created by aligning the blood vessels indicated with arrowheads in Fig. 4, *A–C,* showing the entire penetration. The penetration passed through two blobs (outlined in gray) and associated interblob regions in layer 2/3 before entering layer 4 (also outlined in gray). Lesions mark the layer 4/5 transition and the end of the penetration in layer 6. A two-dimensional schematic of the track reconstruction is shown in Fig. 4*E*. Recording sites are indicated by tick marks; several recording sites are obscured by the asterisks marking lesion sites. Note that our measurements of the locations of recording sitingrelative to CO blobs or laminar borders were not based on schematics like the one shown here but on complete three-dimensional reconstructions of electrode tracks. Data in this figure and in all other quantitative comparisons are taken only from cells with a distance from CO blob centers that could be determined with certainty.

Figure 4*F* shows plots of orientation, spatial, and temporal
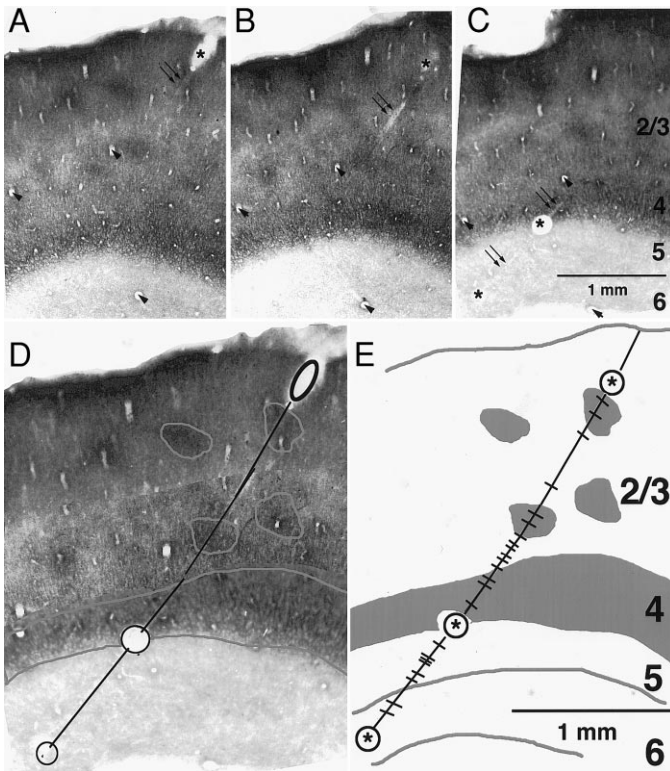
frequency tuning and contrast response recorded from 25 neurons along this track. The first neurons for which we were able to collect quantitative data were located in a blob in the upper part of layer 2/3. Figure 4*F* shows that the receptive field properties of these two neurons and the other two blob neurons recorded in lower layer 2/3 were not obviously different from those of other cells in the upper layers, or other layers of V1. We encountered a number of poorly or nonoriented cells (half-widths $\geq 90°$) along this penetration; however, none of these were located in blobs. We also encountered cells with low-pass spatial frequency tuning; none of these were located in blobs. The cell with the lowest preferred temporal frequency was located in a blob, but there was no trend evident for cells in blobs to prefer lower temporal frequencies than those outside of blobs. Finally, cells in blobs had neither the highest nor the lowest contrast sensitivity of those encountered along this penetration.

In other penetrations, we encountered nonoriented cells in and on the edges of blobs. We also encountered some cells with low-pass spatial frequency tuning in blobs. However, most blob cells did not share those properties; nearby blob cells often had good orientation tuning and band-pass spatial frequency tuning. In some penetrations, blob and edge cells preferred the lowest spatial frequencies, but this trend did not hold up across our sample. Blob and nonblob cells in all penetrations responded over a similar range of temporal frequencies and contrasts. There was considerable heterogeneity in receptive field properties both within and between electrode penetrations.

SIMPLE AND COMPLEX CELLS. We classified V1 neurons as simple or complex on the basis of response modulation to drifting sinusoidal gratings at the optimal spatial frequency. Simple cells responded with modulation at the same temporal frequency as the stimulus. Complex cells responded with an elevation of firing rate, and showed modulation only at low spatial frequencies. We classified cells whose ratio of F1 to DC response at the optimal spatial frequency was >1.0 as simple and cells with an F1:DC ratio <1.0 as complex (Skottun et al. 1991).

Figure 5 shows the distribution of response modulation (at the optimal spatial frequency) for all V1 neurons. It is similar to distributions shown for V1 neurons in other species (Skottun et al. 1991). In our sample, 114 cells (54%)
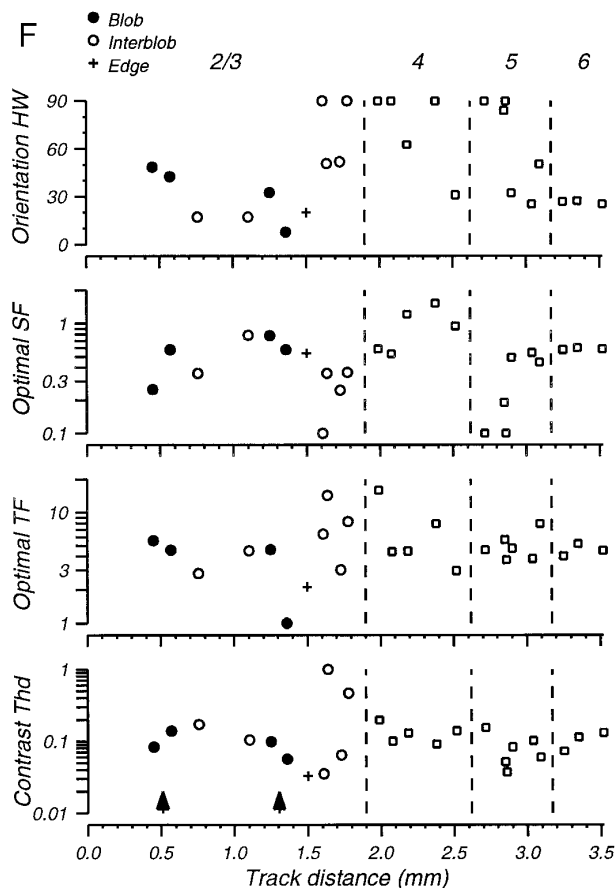
FIG. 4. Example electrode penetration through owl monkey V1. *A*–*C*: photomicrographs of parasagittal sections through V1, stained for cytochrome oxidase (CO). Double arrows indicate visible portions of the electrode track, asterisks indicate locations of electrolytic lesions, and arrowheads indicate the blood vessels aligned in making the montage shown in *D*. Numbers (in *C* and *E*) indicate cortical layers. *D*: montage of the entire electrode penetration made by combining sections shown in *A*–*C*. Line indicates course of the electrode track, whereas oval and circles indicate lesions. Blobs near the electrode track are outlined in gray, as are the borders of layer 4. *E*: schematic representation of the montage in *D*, showing recording sites (tick marks), lesions (asterisks in circles), blobs (in gray), and layer 4 (in gray). *F*: receptive field properties (orientation half-width, optimal spatial frequency, optimal temporal frequency, and contrast threshold) of neurons encountered along the penetration. Numerals identify layers, and vertical dashed lines indicate laminar boundaries. Filled circles indicate data from cells located in blobs, open circles indicate data from cells located in interblob regions, plus signs indicate data from cells located on blob edges, and open squares indicate data from cells in granular and infragranular layers. Upward-pointing arrows (*bottom*) indicate locations of blob centers.
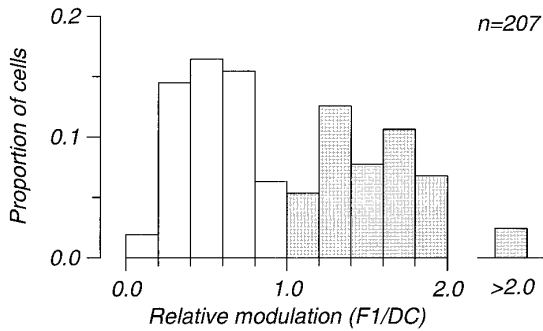
FIG. 5. Distribution of relative modulation ratio (F1:DC) for owl monkey V1 neurons. Neurons with a modulation ratio >1.0 were classified as simple cells. Neurons with a modulation ratio ≤1.0 were classified as complex cells. Other conventions as in Fig. 2.

were classified as complex and 96 were classified as simple (46%).

We found both simple and complex cells in all layers and in all compartments. Roughly equal proportions of simple (48%) and complex (52%) cells were assigned to layer 2/3. Simple cells accounted for 42% of our sample of layer 4 neurons and 28% of our sample of layer 5/6. One-half of the 42 cells that we were not able to assign to layers were classified as simple. Of the 28 cells assigned to blobs, 13 (46%) were classified as simple, 15 as complex. Simple cells accounted for 17 of the 26 cells (65%) assigned to interblobs and 11 of the 17 cells (65%) assigned to edges of blobs.

EYE DOMINANCE. We made qualitative assessment of eye dominance on all 211 neurons using the Hubel and Wiesel (1962) seven-point scale. Figure 6 shows the eye dominance distribution for our sample. Some 22% of the cells were clearly binocular (group 4), whereas only 13% of the cells were clearly monocular. Simple cells were equally likely to be binocular or monocular, whereas complex cells were somewhat more likely to be binocular than monocular.

We found monocularly and binocularly driven neurons equally often in all layers and all compartments. The slight majority of neurons in layers 2/3 was binocularly driven; groups 3, 4, and 5 accounted for 60% of layer 2/3 cells. Within layers 2/3, neurons located in CO blobs were as or
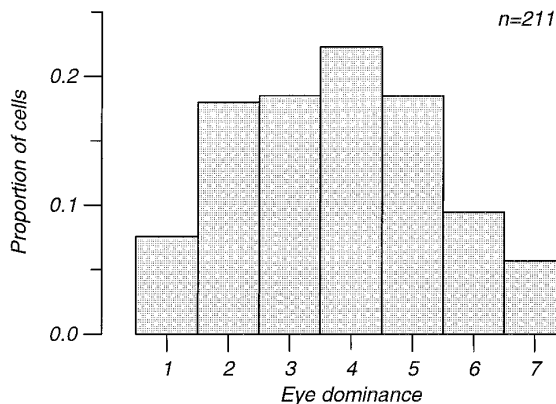

FIG. 6. Eye dominance distribution for owl monkey V1 neurons. Eye dominance of 1 indicates monocular contralateral input, while eye dominance of 4 indicates binocular input. Other conventions as in previous figure.
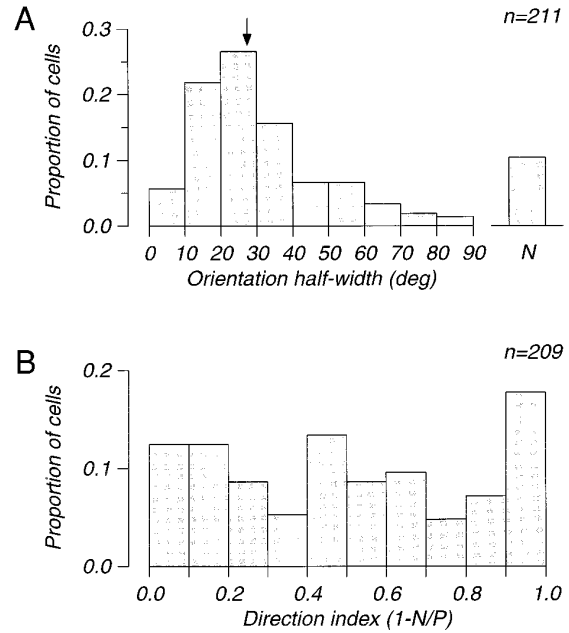

FIG. 7. Orientation and direction selectivity of owl monkey V1 neurons. A: distribution of orientation tuning half-widths. Bin marked N indicates nonoriented cells. B: distribution of direction indices for the same neurons. Cells with a direction index ≥0.67 were classified as direction selective. Other conventions as in previous figures.

more likely to be *binocular* than monocular. Neurons in the granular and infragranular layers were roughly equally often monocular and binocular.

ORIENTATION AND DIRECTION SELECTIVITY. Figure 7A shows the distribution of orientation half-width for our entire V1 sample, and Table 2 lists all quantitative receptive field properties for our sample. Orientation half-widths were similar in simple and complex cells.

We found no significant differences in orientation selectivity for cells assigned to different compartments. All compartments contained nonoriented cells as well as relatively narrowly tuned cells. The receptive field parameters for cells in each compartment are shown in Table 3. Orientation half-widths are plotted in Fig. 8A as a function of the distance (parallel to the cortical surface) from the nearest blob center. It is clear from the figure that the range of orientation tuning was similar across compartments.

The orientation half-widths for cells in each layer are shown in Fig. 8B. Small ticks indicate half-widths for individual neurons and open squares indicate medians for each layer (nonoriented cells were excluded from this computation). The receptive field parameters for cells in each layer are shown in Table 4. There was a broad range of orientation selectivity across layers—all layers contained nonoriented cells and all layers contained at least some relatively narrowly tuned cells. We compared orientation half-widths for cells in layers 2/3, 4, and 5/6 using the Kruskal-Wallis ANOVA by ranks and found no significant differences among layers.

The distribution of direction indices for our entire V1 sample is shown in Fig. 7B. Nearly one-third of the cells in the sample were classified as direction selective. We found direction-selective cells in all compartments, although we

TABLE 2. *Summary of receptive field properties for all cells in our V1 sample*

Property	Overall	Simple	Complex	P
Spatial tuning				
Orientation half-width, deg	27.4 (189)	30.8 (79)	26.9 (110)	0.0289
Optimal spatial frequency, cycles/deg	0.71 (199)	0.61 (88)	0.79 (111)	**<0.001**
Spatial resolution, cycles/deg	2.67 (207)	2.0 (95)	3.0 (112)	**<0.001**
Spatial bandwidth (octaves)	2.1 (186)	2.0 (78)	2.1 (108)	0.1552
Temporal tuning				
Optimal temporal frequency, Hz	3.0 (185)	3.4 (87)	2.7 (98)	0.0540
Temporal resolution, Hz	10.3 (195)	10.6 (92)	10.3 (103)	0.4378
Temporal bandwidth (octaves)	3.8 (185)	3.7 (92)	3.7 (104)	0.2039
Contrast response				
Peak response, imp/s	18.6 (202)	16.2 (90)	22.4 (112)	**0.0017**
Contrast at half-peak response (C_{50})	0.42 (202)	0.42 (90)	0.42 (112)	0.4653
Contrast threshold	0.14 (195)	0.15 (85)	0.13 (110)	0.0519
Peak responsivity (at contrast $\leq$0.2)	20.4 (202)	19.0 (90)	22.9 (112)	0.4727

Values are medians; number of cells in parentheses. *P* values based on the nonparametric Mann-Whitney *U* test; *P* values in boldface indicate significance at the 0.01 level.

found fewer in blobs (3/28 or 11%) than in edge (8/17 or 47%) or interblob (10/26 or 38%) compartments. This difference was marginally significant ($\chi^2 = 8.26$, df = 2, $P < 0.016$) and might also be meaningful. All layers contained both direction-selective neurons and nonselective neurons. Overall, 30% (30 of 100) of layer 2/3 neurons, 44% (23 of 52) of layer 4 neurons, and 22% (4 of 18) of layer 5/6 neurons were classified as direction selective.

SPATIAL FREQUENCY TUNING. V1 neurons generally exhibited band-pass spatial frequency tuning like that shown in Fig. 3, *B* and *F*. A minority of the sample (21/207) showed low-pass tuning (i.e., the responses to the lowest spatial frequencies tested were at least one-half the response to the optimal spatial frequency). Distributions of spatial frequency tuning parameters (optimal spatial frequency, spatial resolution, and spatial tuning bandwidth) are shown in Fig. 9. Complex cells had significantly higher optimal spatial frequencies ($P < 0.006$) and spatial resolutions ($P < 0.0001$) than did simple cells. Complex and simple cells had similar spatial tuning bandwidths.

We measured spatial frequency tuning for 25 of 28 cells assigned to blobs and for all cells assigned to edges (17) and interblobs (26). We found cells with low-pass spatial tuning in all compartments. There were no significant differences in spatial frequency tuning for neurons assigned to different compartments. This is illustrated in Fig. 8*C,* which shows optimal spatial frequency as a function of distance to the nearest blob center for all cells assigned to a compartment, and in Table 3. The optimal spatial frequencies were 0.58 cycles/deg for blobs, 0.87 cycles/deg for edges, and 0.78 cycles/deg for interblobs. It is clear that neurons in all compartments responded over a similar range of spatial frequencies.

There were significant differences in optimal spatial frequency across layers. Figure 8*D* shows the optimal spatial frequencies for individual neurons and medians for each layer. Again, we made statistical comparisons between layers 2/3, 4, and 5/6 using the nonparametric Kruskal-Wallis ANOVA by ranks. The optimal spatial frequencies of layer 2/3 cells (0.79 cycles/deg) were significantly ($P < 0.0014$) higher than those of layer 4 or layer 5/6 cells. Neither spatial resolution nor spatial bandwidth showed significant laminar variation (see Table 4).

TEMPORAL FREQUENCY TUNING. Most V1 neurons (95%) exhibited broad bandpass temporal tuning like that shown in Fig. 3*C*. A minority of V1 neurons (10/195) showed low-pass temporal frequency tuning like that illustrated in Fig.

TABLE 3. *Comparison of receptive field properties for all cells assigned to CO compartments*

Property	Total	Blob	Edge	Interblob	P
Spatial tuning					
Orientation half-width, deg	26.9 (64)	28.8 (26)	21.4 (15)	19.8 (23)	0.2934
Optimal spatial frequency, cycles/deg	0.78 (64)	0.58 (23)	0.86 (16)	0.78 (25)	0.4016
Spatial resolution, cycles/deg	2.6 (68)	2.5 (25)	2.6 (17)	2.9 (26)	0.5150
Spatial bandwidth (octaves)	2.0 (60)	2.1 (20)	2.2 (15)	2.0 (25)	0.6514
Temporal tuning					
Optimal temporal frequency, Hz	2.1 (56)	1.7 (18)	1.9 (15)	2.6 (23)	0.2021
Temporal resolution, Hz	7.9 (62)	7.8 (21)	7.2 (16)	11.2 (25)	0.4903
Temporal bandwidth (octaves)	3.9 (56)	4.0 (18)	3.5 (15)	4.2 (23)	0.4933
Contrast response					
Peak response, imp/s	18.6 (67)	18.6 (24)	19.5 (17)	17.4 (26)	0.4766
Contrast at half-peak response (C_{50})	0.47 (67)	0.48 (24)	0.49 (17)	0.45 (26)	0.7570
Contrast threshold	0.15 (64)	0.15 (23)	0.13 (17)	0.16 (24)	0.7917
Peak responsivity (at contrast $\leq$0.2)	10.7 (67)	7.9 (24)	12.9 (17)	10.5 (26)	0.9965

Values are medians; number of cells in parentheses. *P* values based on the nonparametric Kruskal-Wallis test; *P* values in boldface indicate significance at the 0.01 level. CO, cytochrome oxidase.
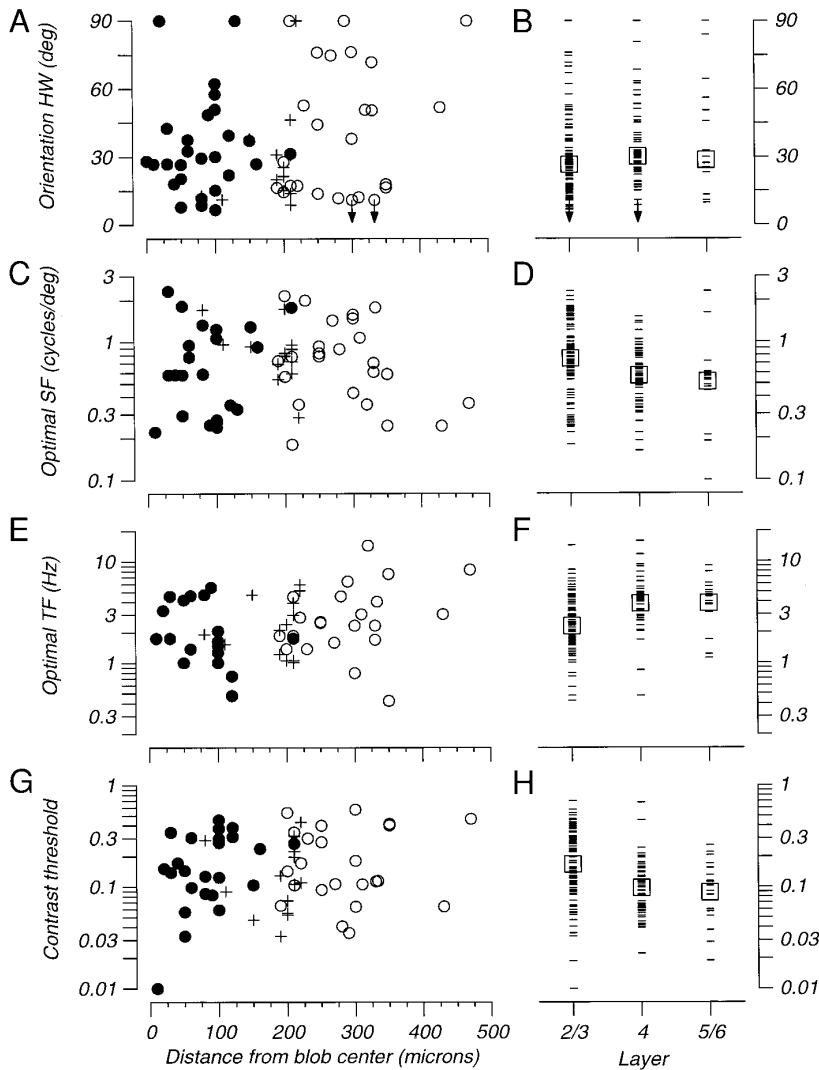
FIG. 8. Horizontal and laminar organization of receptive field properties. *A, C, E,* and *G*: receptive field properties plotted as a function of distance to the center of the nearest blob. Filled circles indicate cells located within blobs, open circles indicate cells located in interblob regions, and plus signs indicate cells located on the edges of blobs. *A*: orientation half-width. Arrows indicate cells that responded to one test orientation only, and therefore had unknown half-widths of ≤11°. *B*: optimal spatial frequency. *C*: optimal temporal frequency. *D*: contrast threshold. *B, D, F,* and *H*: laminar distribution of receptive field properties. Small dashes indicate individual values, open squares indicate medians. *B*: orientation half-width. Arrows as in *A*. *D*: optimal spatial frequency. *F*: optimal temporal frequency. *H*: contrast threshold.

3G. The distribution of temporal frequency tuning parameters (optimal temporal frequency, temporal resolution, and temporal tuning bandwidth) for our sample is shown in Fig. 10.

We measured temporal frequency tuning for 22 (of 28) blob cells, for all edge cells, and for 25 (of 26) interblob cells. Cells with low-pass temporal tuning were encountered in all compartments. Although the cells with the highest

TABLE 4. *Comparison of receptive field for all cells assigned to layers*

Property	Total	Layer 2/3	Layer 4	Layer 5/6	*P*
Spatial tuning					
Orientation half-width, deg	27.6 (153)	26.6 (91)	30.3 (46)	28.7 (16)	0.1331
Optimal spatial frequency, cycles/deg	0.66 (160)	0.79 (92)	0.58 (51)	0.56 (17)	**0.001**
Spatial resolution, cycles/deg	2.6 (167)	2.7 (97)	2.0 (52)	3.4 (18)	0.0179
Spatial bandwidth (octaves)	2.1 (150)	2.1 (87)	2.1 (47)	2.4 (16)	0.6514
Temporal tuning					
Optimal temporal frequency, Hz	3.0 (149)	2.3 (83)	4.2 (50)	4.6 (16)	**<0.001**
Temporal resolution, Hz	11.0 (158)	7.9 (89)	14.8 (51)	14.1 (18)	**<0.001**
Temporal bandwidth (octaves)	3.9 (149)	3.8 (83)	3.8 (50)	4.1 (16)	0.4601
Contrast response					
Peak response, imp/s	19.5 (163)	17.0 (95)	25.7 (50)	35.4 (18)	**<0.001**
Contrast at half-peak response (C_{50})	0.41 (163)	0.46 (95)	0.33 (50)	0.34 (18)	**<0.001**
Contrast threshold	0.13 (157)	0.17 (92)	0.10 (47)	0.09 (18)	**<0.001**
Peak responsivity (at contrast ≤0.2)	25.1 (163)	10.2 (95)	42.7 (50)	58.9 (18)	**<0.001**

Values are medians; number of cells in parentheses. *P* values based on the nonparametric Kruskal-Wallis test; *P* values in boldface indicate significance at the 0.01 level.
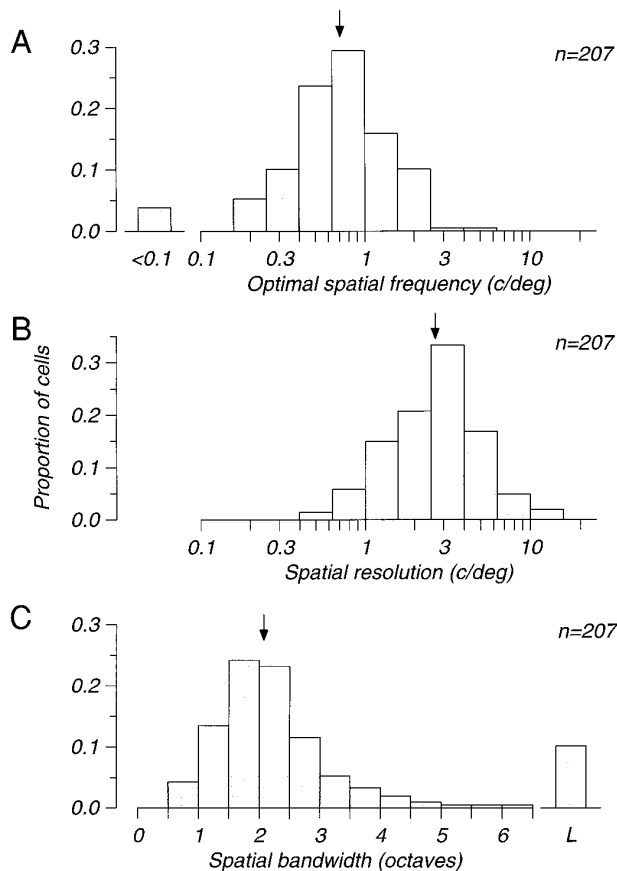
FIG. 9. Spatial frequency selectivity of owl monkey V1 neurons. *A*: distribution of optimal spatial frequencies. *B*: distribution of spatial resolutions. *C*: distribution of spatial tuning bandwidths. Bin marked L indicates cells with ''low-pass'' spatial tuning. Other conventions as in previous figures.

optimal temporal frequencies were in interblobs, there were no significant differences in temporal frequency tuning for cells assigned to the different compartments. The optimal temporal frequencies for neurons in all compartments are shown plotted as a function of distance from blob centers in Fig. 8*E*. Temporal frequency tuning parameters are also summarized in Table 3.

Temporal frequency tuning did vary significantly across layers. The optimal temporal frequencies across layers are shown in Fig. 8*F* and Table 4. The optimal temporal frequency of neurons in layers 2/3 was significantly lower ($P < 0.0001$) than that of neurons in layers 4 or 5/6. The temporal resolution of neurons in layers 2/3 was also significantly ($P < 0.0001$) lower than that of neurons in layers 4 or 5/6. Cells with low-pass temporal tuning were somewhat more frequently encountered in layers 2/3 (7) than in layers 4 (1) or 5/6 (2).

CONTRAST RESPONSE. Distributions of the contrast-response parameters (peak, C_{50}, threshold) for our sample are shown in Fig. 11.

We measured contrast response for 24 of 28 cells assigned to blobs and for all cells assigned to edge and interblob regions. There were no significant differences in any of the measures of contrast sensitivity for cells assigned to different compartments. For example, Fig. 8*G* shows contrast thresh-

old as a function of distance to the nearest blob center; no trend is evident. The most sensitive cell of our entire V1 sample was located in a blob, but it is clear that cells in all compartments responded over similar ranges of contrast (see Table 3).

There were significant laminar differences in contrast sensitivity. Figure 8*H* shows contrast thresholds for neurons in each layer. The median contrast threshold for neurons in layer 2/3 was significantly higher ($P < 0.0001$) than that for neurons in layers 4 or layers 5/6. The peak response also varied significantly ($P < 0.0001$) across layers, summarized in Table 4.

In our LGN data, the largest difference between M and P cells was in responsivity (the initial slope of the contrast-response function). We wondered if there were differences in the responsivity of V1 neurons in different compartments or layers. Because of the inherent nonlinearity in V1 contrast response, we could not compute responsivity in the same way we did for LGN neurons. Instead, for each cell, we computed ''peak responsivity,'' the maximum slope of the contrast-response function at the low contrasts (≤ 0.2) at which M and P cells differ most in responsivity. Log peak responsivity was inversely correlated with log contrast threshold ($r = -0.768$, $P < 0.001$); cells with high peak responsivity tended to have low thresholds. There was no significant difference in peak responsivity between compart-
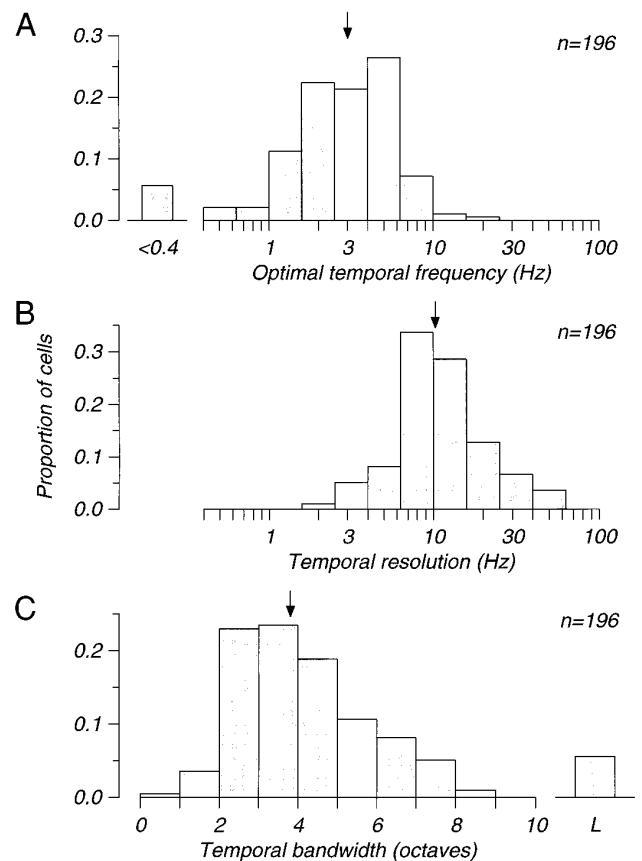

FIG. 10. Temporal frequency selectivity of owl monkey V1 neurons. *A*: distribution of optimal temporal frequencies. *B*: distribution of temporal resolutions. *C*: distribution of temporal tuning bandwidths. Bin marked L indicates cells with ''low-pass'' temporal tuning. Other conventions as in previous figures.
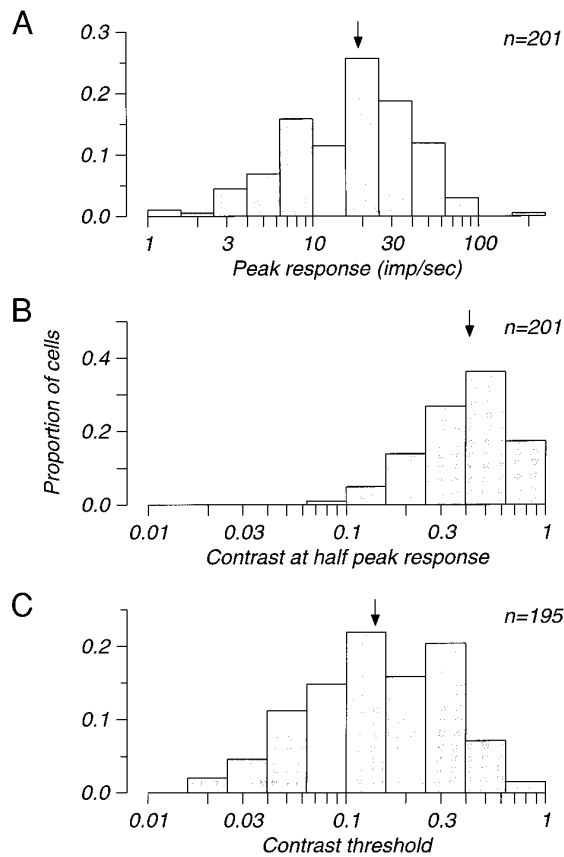
A

B

C

FIG. 11. Contrast sensitivity of owl monkey V1 neurons. *A*: distribution of peak response (response at unit contrast in imp/s). *B*: distribution of C_{50}, the contrast evoking half-peak response. *C*: distribution of contrast threshold. Conventions as in previous figures.

ments (see Table 3), but there was a significant difference between layers (see Table 4): cells in layer 2/3 had significantly lower peak responsivity ($P < 0.001$) than those in layers 4 and 5/6. Finally, we measured maintained discharge (firing rate in absence of a visual target). We found no significant variation in maintained discharge across either compartment or layer.

We wondered if the surprisingly low contrast sensitivity we observed in owl monkey V1 might be due to luminance saturation of a rod-dominated retina—we made measurements at a luminance level where cones were more sensitive than rods (Jacobs 1977). Our qualitative impression was that responses differed little over a wide range (2 log units) of mean luminance. These impressions were supported by a small number of quantitative experiments. We collected contrast-response functions for five cells in one monkey before and after placing a 2 log unit neutral density filter in front of the tested eye. In each case, the nontested eye was occluded, and we waited ≥10 min for the tested eye to adapt to the lower mean luminance. The 100-fold reduction brought the luminance into the range where owl monkey rods and cones have similar sensitivity but had little effect on contrast response. Two cells showed slightly larger peak responses and lower C_{50}'s at lower luminance, whereas three cells showed the opposite effects. We concluded that the poor contrast sensitivity we observed was not due to rod saturation.

DISCUSSION

Receptive field properties of owl monkey LGN

We examined receptive field properties in the LGN to determine if the achromatic properties of the magnocellular and parvocellular pathways in the owl monkey are similar to those found in other primates. Our results show that the owl monkey has magnocellular and parvocellular neurons that differ in the same ways as homologous neurons do in other primates. Neurons in the parvocellular layers of owl monkey LGN tended to have smaller receptive field centers, lower optimal temporal frequencies, and lower responsivity than neurons in the magnocellular layers. The differences in receptive field center size reported here may be contaminated by eccentricity effects. In macaques, the center size of M and P cells from matched eccentricities were similar, although P cells generally had the smallest centers (Derrington and Lennie 1984; Levitt et al. 1989; Spear et al. 1994). On the other hand, measurements made in the LGN of the nocturnal prosimian bush baby indicate that M cell receptive field centers were twice as large as P cell receptive field centers across eccentricity (Irvin et al. 1993), a finding consistent with our data. Receptive field sizes of owl monkey LGN neurons were larger than those of the macaque by a factor of about 2 (Derrington and Lennie 1984; Levitt et al. 1989; Spear et al. 1994) and smaller than those of the bush baby by a factor of about 2 (Irvin et al. 1993; Norton and Casagrande 1982; Norton et al. 1988). The differences in owl and macaque monkey RF size may reflect differences in relative cone density—the owl monkey has half the number of cones per degree of visual angle than the macaque (Wikler and Rakic 1990).

The temporal frequency tuning of most owl monkey LGN neurons, as in macaque, was band-pass, though owl monkey LGN neurons generally had sharper low frequency roll-offs than in macaque (Levitt et al. 1989). Owl monkey LGN cells responded over a range of temporal frequencies lower than macaque LGN cells, (Derrington and Lennie 1984; Hawken et al. 1996; Spear et al. 1994) but higher than bush baby LGN cells (Norton et al. 1988).

The contrast-response properties of owl monkey LGN cells were broadly similar to those of macaque LGN cells, but the difference between owl monkey M and P cell responsivity (or contrast gain) was smaller than the differences reported for macaque M and P cells (Kaplan and Shapley 1982; Levitt et al. 1989; Spear et al. 1994). The smaller difference is due to the relative insensitivity of owl monkey M cells. This suggests that it might be difficult to see a clear sensitivity ''signature'' of M or P cell input to owl monkey cortical neurons. The spatial and temporal properties of owl monkey LGN cells were surprisingly similar to those of the macaque, given the large phylogenetic and niche differences.

Receptive field properties of owl monkey V1

Owl monkey V1 receptive fields were similar to those found in other primates. Most neurons were orientation selective, were band-pass in spatial and temporal frequency tuning and had saturating contrast-response functions (see chapter 4 in De Valois and De Valois 1990). We first compare briefly the receptive field properties of owl monkey

V1 neurons with those of the diurnal Old World macaque monkey, as this is the species from which most of the data on blob anatomy and physiology is based, and with those of the nocturnal prosimian bush baby, an animal that shares a similar ecological niche (DeBruyn et al. 1993).

The eye dominance distribution for the owl monkey was more binocular that of macaque (Hubel and Wiesel 1968) and the nocturnal prosimian bush baby but similar to that of squirrel monkey (Livingstone and Hubel 1984). The small proportion of monocular cells in our sample is consistent with the weak expression of eye dominance columns in the geniculocortical projections of the owl monkey (Diamond et al. 1985; Kaas et al. 1976; Rowe et al. 1978). We note also that the squirrel monkey has indistinct ocular dominance columns that are not in register with the CO blobs (Horton and Hocking 1996). Owl monkey V1 neurons were more sharply tuned for orientation than macaque V1 neurons but more broadly tuned than bush baby cortical neurons. We found fewer nonoriented cells than in macaque (De Valois et al. 1982a) but more than in bush baby. About one-third of the cells in the current sample were direction selective within the range reported for macaque (De Valois 1982b; Schiller et al. 1976) but greater than that reported for bush baby (DeBruyn et al. 1993). The proportion of direction-selective cells was surprisingly high (given our upper-layer sampling bias) compared with the macaque (Hawken et al. 1988) but was consistent with the report of direction-selective cells in all layers of V1 of the marmoset, another New World primate (Sengpiel et al. 1996). The optimal spatial frequencies of owl monkey V1 cells were some five times lower and bandwidths were somewhat wider than those reported in macaque (De Valois et al. 1982a). Optimal spatial frequency was similar, and bandwidth narrower, in owl monkey than in bush baby V1 cells. Like the macaque, but unlike the bush baby, owl monkey simple and complex cells had similar spatial bandwidths. Owl monkey V1 cells responded over a lower range of temporal frequencies than macaque V1 cells, though the drop in optimal temporal frequency between the LGN and V1 in owl monkey was similar to that in macaque (Hawken et al. 1996). The temporal tuning of owl monkey V1 cells was more band-pass than those in bush baby. The contrast sensitivity of owl monkey V1 cells was much poorer than that of macaque V1 cells (Albrecht and Hamilton 1982; Sclar et al. 1990) and also substantially poorer than those of the bush baby (which were reported to be similar to macaque).

Functional organization of owl monkey V1

SIMILARITY IN RECEPTIVE FIELD PROPERTIES ACROSS COMPARTMENTS.   Our most striking finding was negative: there was no important variation in receptive field properties across CO compartments. We found no differences in cell type, eye dominance, spatial tuning, temporal tuning, or contrast response in different compartments; blob compartments had fewer direction-selective neurons than the other compartments. It is of course possible that receptive field properties within compartments might vary with cortical depth, but our sample of cells was too small to examine this possibility. Our conclusions are based on data from 71 neurons. We might have preferred larger samples from each compartment

but elected to make extensive quantitative measurements of receptive field properties of each recorded neuron instead of making qualitative estimates from a larger number of cells. Had there been consistent differences in properties of neurons in different V1 compartments, we certainly would have observed them. This suggests that variations in receptive field properties across different compartments are either absent or too subtle to be revealed by a sample of this size. Of course, it is possible that neurons in different compartments differ in ways that we did not measure. For example, we made no effort to assess the chromatic properties of owl monkey cells because all evidence suggests that owl monkeys have very poor color vision (Jacobs 1977; Jacobs et al. 1993; Kemp and Jacobson 1991; Wikler and Rakic 1990).

V1 in the owl monkey does not appear to exhibit the kind of segregation of receptive field properties across compartments reported for macaque V1. Livingstone and Hubel (1984, p. 309) suggested that cells in macaque blobs formed a color system ''parallel to and separate from the orientation-specific system.'' It also has been suggested that cells in blobs are monocular (Livingstone and Hubel 1984), color-opponent (Livingstone and Hubel 1984; Ts'o and Gilbert 1988), prefer low spatial frequencies (Born and Tootell 1991; Edwards et al. 1995; Silverman et al. 1989), and have high contrast sensitivity (Hubel and Livingstone 1990; Tootell et al. 1988b). Some of these distinctions appeared to be less sharp than first claimed; Lennie et al. (1990) examined chromatic properties in macaque V1 neurons; they found no evidence for segregation of chromatic properties within the cytochrome oxidase blobs. Leventhal et al. (1995) examined properties of neurons in the upper layers of macaque V1 and found a broad range of orientation, chromatic, and direction selectivity in layers 2/3 that was unrelated to the pattern of cytochrome oxidase staining. Furthermore, they found no overall relationship between chromatic sensitivity and orientation selectivity. They did find that cells with high chromatic sensitivity had lower optimal spatial frequencies than those with low chromatic sensitivity and exhibited poorer orientation selectivity when tested with bars (but not when tested with gratings), suggesting that earlier studies with bar stimuli may have underestimated the orientation selectivity of color-sensitive cells (Leventhal et al. 1995).

The monocularity of macaque blob cells is consistent with the observation that, in this species, blobs are aligned with eye dominance columns (Horton 1984). However, it is not clear that blobs and eye dominance columns are aligned in all primates; Horton and Hocking (1996) showed that the New World squirrel monkey has ''indistinct'' eye dominance columns but that there was no consistent relationship between the centers of eye dominance columns and CO blobs. We found no relationship between neuronal eye dominance and CO blobs in the owl monkey. The owl monkey also has an indistinct pattern of eye dominance columns (Diamond et al. 1985; Kaas et al. 1976; Rowe et al. 1978), and it seems likely that there is no relationship between the CO blobs and eye dominance columns in this species.

There appears to be some segregation of spatial frequency tuning in macaque visual cortex. Several studies have found that cells within blobs preferred lower spatial frequencies

than cells in interblob regions (Born and Tootell 1991; Edwards et al. 1995; Silverman et al. 1989; Tootell et al. 1988c). In our own data, there was a weak tendency for cells in blobs to have lower optimal spatial frequencies and resolutions than edge and interblob cells, but this was far from approaching statistical significance. In macaque, Leventhal et al. (1995) found no significant differences in spatial tuning for blob and interblob cells, and DeBruyn et al. (1993) found in bush baby that cells in blobs had *higher* optimal spatial frequencies than interblob cells.

The pattern of geniculocortical and intracortical connections in primates (reviewed in Casagrande 1994; Casagrande and Kaas 1994; Lund et al. 1994) suggests that blob and interblob regions may receive different patterns of M and P inputs. One might expect neurons in regions that receive magnocellular input to have better contrast sensitivity than neurons that receive parvocellular input. Blobs in primate visual cortex do receive direct projections from the LGN, but from the intercalated/koniocellular layers (depending on the species) (see Casagrande 1994). The M and P inputs to blobs are indirect; in owl monkeys, blobs appear to receive mixed inputs from M and P recipient layers, whereas interblob regions appear to receive relatively greater input from M recipient layers (Casagrande and Kaas 1994; Casagrande et al. 1992). We saw no sign of this in the contrast-response of V1 neurons—there were no significant differences in contrast sensitivity in different CO compartments. However, we saw clear signs of magnocellular input in the contrast-response properties of layer 4 neurons (most of which were in the upper, M-recipient layer), which had, on average, significantly higher contrast sensitivity than those in the upper or lower layers.

In macaque monkeys, the (indirect) M and P inputs to layers 2/3 are different from those in the owl monkey, with blobs receiving relatively heavier M pathway input than interblob regions (Callaway and Wiser 1996; Lachica et al. 1992, 1993; Yoshioka et al 1994). Hubel and Livingstone (1990) examined contrast sensitivity of macaque LGN and V1 cells but found no clear differences in contrast sensitivity between neurons located in blob and interblob regions. They reported that most layer 2/3 neurons had better contrast sensitivity than the parvocellular inputs to V1. Edwards et al. (1995) found that only neurons near the centers of blobs in macaque V1 had contrast sensitivity approaching that of magnocellular inputs with the rest of layer 2/3 neurons exhibiting contrast sensitivity similar to that of parvocellular inputs, a pattern thought to be consistent with the relative density of the M and P projections. In bush baby, cells in blobs had *lower* contrast sensitivity than cells in interblob regions, consistent with relatively heavier magnocellular input to interblobs (DeBruyn et al. 1993). We found no significant difference in any measure of contrast sensitivity across compartments. Perhaps this was because the differences in M and P cell contrast sensitivity are less pronounced than in macaque.

Alternatively, the anatomic segregation of the M and P pathways may not be reflected in the physiology; the physiological evidence suggests considerable mixing of signals in V1 (Malpeli et al. 1981; Nealey and Maunsell 1994; Sawatari and Callaway 1996). It is also important to consider that the receptive field properties in the blobs might reflect

neither M or P input but depend instead on the direct inputs from the interlaminar or koniocellular (K) thalamocortical pathway (Casagrande 1994). Unfortunately little is known at present about the receptive field properties of K neurons in monkeys. In the prosimian bush baby, K and interlaminar cells formed a separate functional class with long response latency, low firing rate, and heterogeneous receptive field organization. The relatively small proportion of K cells that had standard center-surround organization had spatial and contrast sensitivity properties that fell between those of M and P cells (Irvin et al. 1986, 1993; Norton and Casagrande 1982; Norton et al. 1988). If this pathway does provide a major input to CO blobs, the differences observed between macaque and owl monkey CO blobs might reflect differences in the K pathway between these species.

Differences in receptive field properties across layers

Although we found no clear differences in the properties of neurons in different CO compartments, we did find significant differences in receptive field properties across layers. Neurons in the supragranular layers had higher optimal spatial frequencies, lower temporal resolution, and were less responsive and had lower contrast sensitivity than cells in the granular and infragranular layers. Our sample of layer 4 cells was heavily biased—92% of our 52 layer 4 cells were located in the upper, magnocellular-recipient sublayer. Thus it should be no surprise that the spatial, temporal, and contrast-response properties of our layer 4 cells were more similar to M LGN cells than were those of upper layer cells.

One property that does appear to be differently distributed in owl monkey and macaque V1 is direction selectivity. In macaque, direction-selective neurons appear to be limited to the upper parts of layer 4 and layer 6 (Hawken et al. 1988; Hubel and Livingstone 1990). In the owl monkey, we found direction-selective neurons in all cortical layers, including the upper parts of layers 2/3 and layer 5, as did Sengpiel et al. (1996) in marmoset V1. The laminar organization of receptive field properties appears to be different in owl monkey and bush baby. In bush baby, supragranular layers have higher contrast sensitivity, higher optimal temporal frequencies, and lower optimal spatial frequencies than the infragranular layers (DeBruyn et al. 1993). We found the opposite pattern in the owl monkey, though our small sample of infragranular cells compels a cautious interpretation of this result.

REFERENCES

ALBRECHT, D. G. AND HAMILTON, D. B. Striate cortex of monkey and cat: contrast response function. *J. Neurophysiol.* 48: 217–237, 1982.

ALLMAN, J. M. AND KAAS, J. H. Representation of the visual field in striate and adjoining cortex of the owl monkey (*Aotus trivirgatus*). *Brain Res.* 35: 89–106, 1971a.

ALLMAN, J. M. AND KAAS, J. H. A representation of the visual field in the caudal third of the middle tempral gyrus of the owl monkey (*Aotus trivirgatus*). *Brain Res.* 31: 85–105, 1971b.

ALLMAN, J. M. AND KAAS, J. H. A crescent-shaped cortical visual area surrounding the middle temporal area (MT) in the owl monkey (*Aotus trivirgatus*). *Brain Res.* 81: 199–213, 1974a.

ALLMAN, J. M. AND KAAS, J. H. The organization of the second visual area (V II) in the owl monkey: a second order transformation of the visual hemifield. *Brain Res.* 76: 247–265, 1974b.

ALLMAN, J. M. AND KAAS, J. H. The dorsomedial cortical visual area: a third tier area in the occipital lobe of the owl monkey (*Aotus trivirgatus*). *Brain Res.* 100: 473–487, 1975.

BORN, R. T. AND TOOTELL, R. B. Spatial frequency tuning of single units in macaque supragranular striate cortex. *Proc. Natl. Acad. Sci. USA* 88: 7066–7070, 1991.

CALLAWAY, E. M. AND WISER, A. Contributions of individual layer 2–5 spiny neurons to local circuits in macaque primary visual cortex. *Vis. Neurosci.* 13: 907–922, 1996.

CASAGRANDE, V. A. A third parallel visual pathway to primate area V1. *Trends Neurosci.* 17: 305–310, 1994.

CASAGRANDE, V. A. AND KAAS, J. H. The afferent, intrinsic, and efferent connections of primary visual cortex in primates. In: *Cerebral Cortex. Primary Visual Cortex in Primates,* edited by A. Peters and K. S. Rockland. New York: Plenum, 1994, vol. 10, p. 201–259.

CASAGRANDE, V. A., MAVITY-HUDSON, J. A., AND TAYLOR, J. G. Intrinsic connections of owl monkey cortex: difference between cytochrome oxidase (CO) blobs and interblobs. *Soc. Neurosci. Abstr.* 18: 389, 1992.

CONDO, G. J. AND CASAGRANDE, V. A. Organization of cytochrome oxidase staining in the visual cortex of nocturnal primates (*Galago crassicaudatus* and *Galago senegalensis*). I. Adult patterns. *J. Comp. Neurol.* 293: 632–645, 1990.

DEBRUYN, E. J., CASAGRANDE, V. A., BECK, P. D., AND BONDS, A. B. Visual resolution and sensitivity of single cells in the primary visual cortex (V1) of a nocturnal primate (Bush Baby): correlations with cortical layers and cytochrome oxidase patterns. *J. Neurophysiol.* 69: 3–18, 1993.

DE VALOIS, R. L., ALBRECHT, D. G., AND THORELL, L. G. Spatial frequency selectivity of cells in macaque visual cortex. *Vision Res.* 22: 545–559, 1982a.

DE VALOIS, R. L. AND DE VALOIS, K. K. *Spatial Vision*. New York: Oxford, 1990.

DE VALOIS, R. L., YUND, E. W., AND HEPLER, N. The orientation and direction selectivity of cells in macaque visual cortex. *Vision Res.* 22: 531–544, 1982b.

DERRINGTON, A. M., KRAUSKOPF, J., AND LENNIE, P. Chromatic mechanisms in lateral geniculate nucleus of macaque. *J. Physiol. (Lond.)* 357: 241–265, 1984.

DERRINGTON, A. M. AND LENNIE, P. Spatial and temporal contrast sensitivities of neurones in lateral geniculate nucleus of macaque. *J. Physiol. (Lond.)* 357: 219–240, 1984.

DIAMOND, I. T., CONLEY, M., ITOH, K., AND FITZPATRICK, D. Laminar organization of geniculocortical projections in *Galago senegalensis* and *Aotus trivirgatus*. *J. Comp. Neurol.* 242: 584–610, 1985.

EDWARDS, D. P., PURPURA, K. P., AND KAPLAN, E. Contrast sensitivity and spatial frequency response of primate cortical neurons in and around the cytochrome oxidase blobs. *Vision Res.* 35: 1501–1523, 1995.

ENROTH-CUGELL, C. AND ROBSON, J. G. The contrast sensitivity of retinal ganglion cells in the cat. *J. Physiol. (Lond.)* 187: 517–552, 1966.

GEGENFURTNER, K. R., KIPER, D. C., AND FENSTEMAKER, S. B. Processing of color, form, and motion in macaque V2. *Vis. Neurosci.* 13: 161–172, 1996.

HASSLER, R. Comparative anatomy of central visual systems in day- and night-active primates. In: *Evolution of the Forebrain,* edited by R. Hassler and H. Stephan. New York: Plenum, 1994, p. 419–434.

HAWKEN, M. J. AND PARKER, A. J. Spatial properties of neurons in the monkey striate cortex. *Proc. R. Soc. Lond. B Biol. Sci.* 231: 251–288, 1987.

HAWKEN, M. J., PARKER, A. J., AND LUND, J. S. Laminar organization and contrast sensitivity of direction-selective cells in the striate cortex of the Old World monkey. *J. Neurosci.* 8: 3541–3548, 1988.

HAWKEN, M. J., SHAPLEY, R. M., AND GROSOF, D. H. Temporal frequency selectivity in monkey visual cortex. *Vis. Neurosci.* 113: 477–492, 1996.

HORTON, J. C. Cytochrome oxidase patches: a new cytoarchitectonic feature of monkey visual cortex. *Philos. Trans. R. Soc. Lond. B Biol. Sci.* 304: 199–253, 1984.

HORTON, J. C. AND HOCKING, D. Anatomical demonstration of ocluar dominance columns in striate cortex of the squirrel monkey. *J. Neurosci.* 16: 5510–5522, 1996.

HORTON, J. C. AND HUBEL, D. H. Regular patchy distribution of cytochrome oxidase staining in primary visual cortex of macaque monkey. *Nature* 292: 762–764, 1981.

HUBEL, D. H. AND LIVINGSTONE, M. S. Color and contrast sensitivity in the lateral geniculate body and primary visual cortex of the macaque monkey. *J. Neurosci.* 10: 2223–2237, 1990.

HUBEL, D. H. AND WIESEL, T. N. Receptive fields, binocular interaction and functional architecture in the cat's visual cortex. *J. Physiol. (Lond.)* 160: 106–154, 1962.

HUBEL, D. H. AND WIESEL, T. N. Receptive fields and functional architecture of monkey striate cortex. *J. Physiol. (Lond.)* 195: 215–243, 1968.

HUBEL, D. H. AND WIESEL, T. N. Sequence regularity and geometry of orientation columns in the monkey striate cortex. *J. Comp. Neurol.* 158: 267–293, 1974.

HUBEL, D. H. AND WIESEL, T. N. Ferrier lecture. Functional architecture of macaque monkey visual cortex. *Proc. R. Soc. Lond. B Biol. Sci.* 198: 1–59, 1977.

HUMPHREY, A. L. AND HENDRICKSON, A. E. Background and stimulus-induced patterns of high metabolic activity in the visual cortex (area 17) of the squirrel and macaque monkey. *J. Neurosci.* 3: 345–358, 1983.

IRVIN, G. E., CASAGRANDE, V. A., AND NORTON, T. T. Center/surround relationships of magnocellular, parvocellular, and koniocellular relay cells in primate lateral geniculate nucleus. *Vis. Neurosci.* 10: 363–373, 1993.

IRVIN, G. E., NORTON, T. T., SESMA, M. A., AND CASAGRANDE, V. A. W-like response properties of interlaminar zone cells in the lateral geniculate nucleus of a primate (*Galago crassicaudatus*). *Brain Res.* 362: 254–270, 1986.

JACOBS, G. H. Visual capacities of the owl monkey (*Aotus trivirgatus*). I. Spectral sensitivity and color vision. *Vision Res.* 17: 811–820, 1977.

JACOBS, G. H., DEEGAN, J. F., DEEGAN, D., NEITZ, J., CROGNALE, M. A., AND NEITZ, M. Photopigments and color vision in the nocturnal monkey, *Aotus*. *Vision Res.* 33: 1773–1783, 1993.

JONES, A. E. The lateral geniculate complex of the owl monkey Aotes trivirgatus. *J. Comp. Neurol.* 126: 171–179, 1966a.

JONES, A. E. Wavelength and intensity effects on the response of single lateral geniculate nucleus units in the owl monkey. *J. Neurophysiol.* 29: 125–138, 1966b.

KAAS, J. H., HUERTA, M. F., WEBER, J. T., AND HARTING, J. K. Patterns of retinal terminations and laminar organization of the lateral geniculate nucleus of primates. *J. Comp. Neurol.* 182: 517–553, 1978.

KAAS, J. H., LIN, C. S., AND CASAGRANDE, V. A. The relay of ipsilateral and contralateral retinal input from the lateral geniculate nucleus to striate cortex in the owl monkey: a transneuronal transport study. *Brain Res.* 106: 371–378, 1976.

KAPLAN, E. AND SHAPLEY, R. M. X and Y cells in the lateral geniculate nucleus of macaque monkeys. *J. Physiol. (Lond.)* 330: 125–143, 1982.

KAPLAN, E. AND SHAPLEY, R. M. The primate retina contains two types of ganglion cells, with high and low contrast sensitivity. *Proc. Natl. Acad. Sci. USA* 83: 2755–2757, 1986.

KEMP, C. M. AND JACOBSON, S. G. The distribution and kinetics of visual pigments in the owl monkey retina. *Exp. Eye Res.* 52: 329–335, 1991.

LACHICA, E. A., BECK, P. D., AND CASAGRANDE, V. A. Parallel pathways in macaque monkey striate cortex: anatomically defined columns in layer III. *Proc. Natl. Acad. Sci. USA* 89: 3566–3570, 1992.

LACHICA, E. A., BECK, P. D., AND CASAGRANDE, V. A. Intrinsic connections of layer III of striate cortex in squirrel monkey and bush baby: correlations with patterns of cytochrome oxidase. *J. Comp. Neurol.* 329: 163–187, 1993.

LENNIE, P., KRAUSKOPF, J., AND SCLAR, G. Chromatic mechanisms in striate cortex of macaque. *J. Neurosci.* 10: 649–669, 1990.

LEVENTHAL, A. G., THOMPSON, K. G., LIU, D., ZHOU, Y., AND AULT, S. J. Concomitant sensitivity to orientation, direction, and color of cells in layers 2, 3, and 4 of monkey striate cortex. *J. Neurosci.* 15: 1808–1818, 1995.

LEVITT, J. B., KIPER, D. C., AND MOVSHON, J. A. Receptive fields and functional architecture of macaque V2. *J. Neurophysiol.* 71: 2517–2542, 1994.

LEVITT, J. B., MOVSHON, J. A., SHERMAN, S. M., AND SPEAR, P. D. Effects of monocular deprivation on macaque LGN (Abstract). *Invest. Opthalmol. Vis. Sci.* 30, Suppl.: 296, 1989.

LINSENMEIER, R. A., FRISHMAN, L. J., JAKIELA, H. G., AND ENROTH-CU-GELL, C. Receptive field properties of X and Y cells in the cat retina derived from contrast sensitivity measurements. *Vision Res.* 22: 1173–1183, 1982.

LIVINGSTONE, M. S. AND HUBEL, D. H. Anatomy and physiology of a color system in the primate visual cortex. *J. Neurosci.* 4: 309–356, 1984.

LIVINGSTONE, M. S. AND HUBEL, D. H. Segregation of form, color, movement, and depth: anatomy, physiology, and perception. *Science* 240: 740–749, 1988.

LUND, J. S., YOSHIOKA, T., AND LEVITT, J. B. Substrates for interlaminar connections in area V1 of macaque monkey cerebral cortex. In: *Cerebral Cortex. Primary Visual Cortex in Primates,* edited by A. Peters and K. S. Rockland. New York: Plenum, 1994, vol. 10, p. 37–60.

MALPELI, J. G., SCHILLER, P. H., AND COLBY, C. L. Response properties of single cells in monkey striate cortex during reversible inactivation of individual lateral geniculate laminae. *J. Neurophysiol.* 46: 1102–1119, 1981.

MERIGAN, W. H. AND MAUNSELL, J. H. How parallel are the primate visual pathways? *Annu. Rev. Neurosci.* 16: 369–402, 1993.

MERRILL, E. G. AND AINSWORTH, A. Glass-coated platinum-plated micro-electrodes. *Med. Biol. Eng.* 10: 662–671, 1972.

MURPHY, K. M., JONES, D. G., AND VAN SLUYTERS, R. C. Cytochrome-oxidase blobs in cat primary visual cortex. *J. Neurosci.* 15: 4196–4208, 1995.

NEALEY, T. A. AND MAUNSELL, J. H. Magnocellular and parvocellular contributions to the responses of neurons in macaque striate cortex. *J. Neurosci.* 14: 2069–2079, 1994.

NORTON, T. T. AND CASAGRANDE, V. A. Laminar organization of receptive-field properties in lateral geniculate nucleus of bush baby (*Galago crassicaudatus*). *J. Neurophysiol.* 47: 715–741, 1982.

NORTON, T. T., CASAGRANDE, V. A., IRVIN, G. E., SESMA, M. A., AND PE-TRY, H. M. Contrast-sensitivity functions of W, X, and Y-like relay cells in the lateral geniculate nucleus of bush baby, Galago crassicaudatus. *J. Neurophysiol.* 59: 1639–1656, 1988.

OGDEN, T. E. The receptor mosaic of *Aotes trivirgatus*: distribution of rods and cones. *J. Comp. Neurol.* 163: 165–183, 1975.

PETERS, A. The organization of the primary visual cortex in the macaque. In: *Cerebral Cortex. Primary Visual Cortex in Primates,* edited by A. Peters and K. S. Rockland. New York: Plenum, 1994, vol. 10, p. 1–35.

ROBSON, J. G. Neural images: the physiological basis of spatial vision. In: *Visual Coding and Adaptability*, edited by C. S. Harris. Hillsdale, NJ: L. Erlbaum, 1980, p. 177–214.

ROWE, M. H., BENEVENTO, L. A., AND REZAK, M. Some observations on the patterns of segregated geniculate inputs to the visual cortex in New World primates: an autoradiographic study. *Brain Res.* 159: 371–378, 1978.

SANDELL, J. H. Nadph diaphorase histochemistry in the macaque striate cortex. *J. Comp. Neurol.* 251: 388–397, 1986.

SAWATARI, A. AND CALLAWAY, E. M. Convergence of magno- and parvo-cellular pathways in layer 4b of macaque primary visual cortex. *Nature* 380: 442–446, 1996.

SCHILLER, P. H., FINLAY, B. L., AND VOLMAN, S. F. Quantitative studies of single-cell properties in monkey striate cortex. I. Spatiotemporal organization of receptive fields. *J. Neurophysiol.* 39: 1288–1319, 1976.

SCHILLER, P. H. AND MALPELI, J. G. Functional specificity of lateral genicu-late nucleus laminae of the rhesus monkey. *J. Neurophysiol.* 41: 788–797, 1978.

SCLAR, G., MAUNSELL, J. H., AND LENNIE, P. Coding of image contrast in central visual pathways of the macaque monkey. *Vision Res.* 30: 1–10, 1990.

SENGPIEL, F., TROILO, D., KIND, P. C., GRAHAM, B., AND BLAKEMORE, C. Functional architecture of area 17 in normal and monocularly deprived marmosets (*Callithrix jacchus*). *Vis. Neurosci.* 13: 145–160, 1996.

SHAPLEY, R. M. Parallel retinocortical channels: X and Y and P and M. In: *Applications of Parallel Processing in Vision*, edited by J. Brannan. New York: Elsevier Science Publishers, 1992, p. 3–36.

SHERMAN, S. M., WILSON, J. R., KAAS, J. H., AND WEBB, S. V. X- and Y-cells. in the dorsal lateral geniculate nucleus of the owl monkey (*Aotus trivirgatus*). *Science* 192: 475–477, 1976.

SILVEIRA, L. C., YAMADA, E. S., PERRY, V. H., AND PICANCO-DINIZ, C. W. M and P retinal ganglion cells of diurnal and nocturnal New-World monkeys. *Neuroreport* 5: 2077–2081, 1994.

SILVERMAN, M. S., GROSOF, D. H., DE VALOIS, R. L., AND ELFAR, S. D. Spatial-frequency organization in primate striate cortex. *Proc. Natl. Acad. Sci. USA* 86: 711–715, 1989.

SKOTTUN, B. C., DE VALOIS, R. L., GROSOF, D. H., MOVSHON, J. A., AL-BRECHT, D. G., AND BONDS, A. B. Classifying simple and complex cells on the basis of response modulation. *Vision Res.* 31: 1079–1086, 1991.

SPEAR, P. D., MOORE, R. J., KIM, C. B., XUE, J. T., AND TUMOSA, N. Effects of aging on the primate visual system: spatial and temporal processing by lateral geniculate neurons in young adult and old rhesus monkeys. *J. Neurophysiol.* 72: 402–420, 1994.

TOLHURST, D. J., MOVSHON, J. A., AND DEAN, A. F. The statistical reliability of signals in single neurons in cat and monkey visual cortex. *Vision Res.* 23: 775–785, 1983.

TOOTELL, R. B., HAMILTON, S. L., AND SILVERMAN, M. S. Topography of cytochrome oxidase activity in owl monkey cortex. *J. Neurosci.* 5: 2786–2800, 1985.

TOOTELL, R. B., HAMILTON, S. L., AND SWITKES, E. Functional anatomy of macaque striate cortex. IV. Contrast and magno-parvo streams. *J. Neurosci.* 8: 1594–1609, 1988b.

TOOTELL, R. B., SILVERMAN, M. S., HAMILTON, S. L., DE VALOIS, R. L., AND SWITKES, E. Functional anatomy of macaque striate cortex. III. Color. *J. Neurosci.* 8: 1569–1593, 1988a.

TOOTELL, R. B., SILVERMAN, M. S., HAMILTON, S. L., SWITKES, E., AND DE VALOIS, R. L. Functional anatomy of macaque striate cortex. V. Spatial frequency. *J. Neurosci.* 8: 1610–1624, 1988c.

TS'O, D. Y. AND GILBERT, C. D. The organization of chromatic and spatial interactions in the primate striate cortex. *J. Neurosci.* 8: 1712–1727, 1988.

WIENCKEN, A. E. AND CASAGRANDE, V. A. The distribution of nadph-diaph-orase/nitric-oxide synthase (NOS) within the layers and functional compartments of primate visual cortex (Abstract). *Invest. Ophthalmol. Vis. Sci.* 37, Suppl. 3: 479, 1996.

WIESEL, T. N. AND HUBEL, D. H. Spatial and chromatic interactions in the lateral geniculate body of the rhesus monkey. *J. Neurophysiol.* 29: 1115–1156, 1966.

WIKLER, K. C. AND RAKIC, P. Distribution of photoreceptor subtypes in the retina of diurnal and nocturnal primates. *J. Neurosci.* 10: 3390–3401, 1990.

WONG-RILEY, M. Changes in the visual system of monocularly sutured or enucleated cats demonstrable with cytochrome oxidase histochemistry. *Brain Res.* 171: 11–28, 1979.

WONG-RILEY, M.T.T. Primate visual cortex: dynamic metabolic organization and plasticity revealed by cytochrome oxidase. In: *Cerebral Cortex. Primary Visual Cortex in Primates,* edited by A. Peters and K. S. Rock-land. New York: Plenum, 1994, vol. 10, p. 141–200.

YOSHIOKA, T., LEVITT, J. B., AND LUND, J. S. Independence and merger of thalamocortical channels within macaque monkey primary visual cortex: anatomy of interlaminar projections. *Vis. Neurosci.* 11: 467–489, 1994.